AIP | Applied Physics Letters

Localized electrical characterization of the giant permittivity effect in CaCu3Ti4O12 ceramics

Patrick Fiorenza, Raffaella Lo Nigro, Corrado Bongiorno, Vito Raineri, Matthew C. Ferarrelli et al.

Citation: Appl. Phys. Lett. **92**, 182907 (2008); doi: 10.1063/1.2919095
View online: http://dx.doi.org/10.1063/1.2919095
View Table of Contents: http://apl.aip.org/resource/1/APPLAB/v92/i18
Published by the American Institute of Physics.

Localized electrical characterization of the giant permittivity effect in $CaCu_3Ti_4O_{12}$ ceramics

Patrick Fiorenza,[1,a)] Raffaella Lo Nigro,[1] Corrado Bongiorno,[1] Vito Raineri,[1] Matthew C. Ferarrelli,[2] Derek C. Sinclair,[2] and Anthony R. West[2]
[1]*Istituto per la Microelettronica e Microsistemi, Consiglio Nazionale delle Ricerche, Stradale Primosole 50, 95121 Catania, Italy*
[2]*Department of Engineering Materials, Sir Robert Hadfield Building, University of Sheffield, Mappin Street, Sheffield S1 3JD, United Kingdom*

(Received 12 February 2008; accepted 11 April 2008; published online 8 May 2008)

Nanoscale imaging of the electrical properties of $CaCu_3Ti_4O_{12}$ ceramics has been performed using scanning impedance microscopy. Two kinds of electrical inhomogeneity are detected, namely, depletion layers at grain boundaries and calcium titanate inclusions, both of which are more resistive than the bulk of the grains. Energy filtered transmission electron microscopy was used to estimate the chemical composition of the inclusions. © *2008 American Institute of Physics*.
[DOI: 10.1063/1.2919095]

The perovskite-related material, $CaCu_3Ti_4O_{12}$ (CCTO), has attracted considerable attention in recent years due to its impressive apparent permittivity value of $\sim 10^4-10^5$ at 1 MHz, which remains constant in the temperature range of $\sim 100-600$ K.[1,2] The effect has been observed in both single crystals and ceramics. It is not clear if this effect is an intrinsic property of the material or if it can be related to extrinsic effects, e.g., point and extended defects, contaminants, electrical domain boundaries within grains, grain boundaries, surface layers, and non-ohmic electrode contacts. All of these extrinsic effects have been proposed to lead to higher than expected permittivity values in different oxide-based ceramics.[3–5] Impedance spectroscopy has revealed CCTO ceramics to be electrically heterogeneous and to consist of semiconducting grains and insulating grain boundaries.[6] In this case, the giant permittivity effect in CCTO ceramics has been explained using the well-known internal barrier layer capacitor (IBLC) model. Although this model works reasonably well for CCTO ceramics, the observation of a giant permittivity effect in CCTO single crystals[2] remains perplexing as grain boundary features should not be present in single crystals. The origin of the effect in single crystals may therefore be related to some other features not observed in the ceramics, e.g., non-ohmic contact, modification of crystal surface composition and/or internal boundary layers associated with defects, twins, dislocations, etc. Furthermore, when the IBLC model is applied to polycrystalline ceramics, the results do not exactly scale with the grain dimension, so other effects should also be included.[7]

The question now arises whether the large dielectric response observed in ceramics is due only to an IBLC effect associated with the grain boundaries or whether there is some contribution from defects, inhomogeneities, etc.,[8–10] on a subgranular scale which can also be present in single crystals. In this context, it is important to study and compare the dielectric properties of single grains in addition to those of the grain boundaries. However, to date, such data have not been produced because of the lack of characterization methods with high lateral resolution.

Here, we report on the capabilities of scanning probe microscopy (SPM)-based techniques to study and compare the electrical characteristics within single grains and across grain boundaries. In particular, we demonstrate a new use of scanning capacitance microscopy, namely scanning impedance microscopy (SIM), to directly image the ceramic microstructure and provide information, with high lateral resolution, on the local electrical properties. By applying a bias between the bottom electrode and the conductive AFM tip which acts, on the sample surface, as a sliding metal contact, it is possible to collect the impedance signal of the nanodevice consisting, in our case, of a tip/CCTO/bottom electrode.

The CCTO ceramic pellets were prepared by the mixed oxide route as described in detail elsewhere.[6] After fabrication, the pellets were polished to eliminate the influence of superficial artifacts in the SPM mapping. Measurements were performed using a back contact, which is obtained by silver paint, which is opposite to the polished surface. Measurements on the nanometer scale were performed by a Digital Instrument D3100 atomic force microscope (AFM) with a nanoscope IIIA controller operating in air and equipped with the tunneling atomic force microscopy module. SIM measurements were carried out in constant ΔV mode. The ac bias applied between the tip and the sample was varied in the $1-10$ V peak-to-peak range at 90 kHz with the resonator frequency of 1.0 ± 0.1 GHz.

The SIM is an ordinary AFM equipped with a conductive tip and connected to a resonator (Fig. 1). The collected SIM signal amplitude is related to the sample impedance. The current flowing through the sample, which is collected at the nanometer scale, can be described by

$$A_{\mathrm{SIM}} = \frac{RV_{\mathrm{hf}}}{\sqrt{[R+\mathrm{Re}(Z^*)]^2 + \left[\left(\omega L - \frac{1}{\omega C}\right) + \mathrm{Im}(Z^*)\right]^2}}, \qquad (1)$$

where R, L, C, ω, and V_{hf} are the characteristics of the resonator circuit, while Z^* is the complex impedance and is modeled by an ideal equivalent circuit consisting of resistors and capacitors.[11]

A SIM map provides simultaneous imaging of both the real and imaginary parts of the complex impedance, as shown by Eq. (1). In particular, the high resistance at the

[a)]Electronic mail: fiorenza@imm.cnr.it.

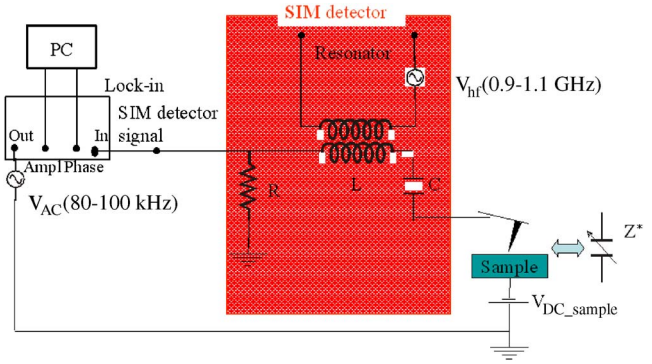

FIG. 1. (Color online) Schematic of the SIM experimental setup. A resonator is connected to the AFM conductive tip and to the lock-in amplifier. The applied oscillating signal can be varied in the range of a few kilohertz. The resonator frequency is fixed at ~1 GHz.

grain boundaries produces an increase of the real part of the impedance and a decrease in the SIM signal amplitude.

Other workers[12,13] have shown the presence of a double Schottky barrier at the grain boundaries; however, the depletion region width has not yet been reported. The depletion region width can be estimated from the ceramic microstructure and from assuming a value for the bulk permittivity, since, according to the simple IBLC model,[14] the ceramic permittivity can be expressed as

$$\varepsilon^* \approx \varepsilon_b \frac{d}{t}, \tag{2}$$

where ε^* is the measured permittivity, ε_b is the intrinsic bulk permittivity, d is the mean grain dimension, and t is the width of the depleted layer at the grain boundaries. Alternatively, if the depletion layer width can be directly measured, the bulk permittivity, for instance, can be calculated.

The experimental value of the permittivity of the CCTO sample used here (mean grain size ~5 μm) is about 7000 at 100 kHz. The depletion width at the grain boundaries is directly observed in the SIM image [Fig. 2(b)] and is estimated to be 130 ± 20 nm, and thus, the bulk permittivity is calculated to be ~160. The value of t is quite different from that of a few nanometers suggested in the literature,[15] however, ε_b is in good agreement with theoretical predictions[16] and direct measurements at low temperature.[6]

The dependence of the depleted region width at the grain boundaries upon the application of ac and dc voltages has also been evaluated. No evident variation in SIM images upon changing the longitudinal applied voltage has been observed. Moreover, several tips with different contact areas and made from two different materials, which are Pt and polycrystalline high conductivity diamond, have been used to exclude any possible electrode-related artifacts.

Finally, the influence of grain size on the grain boundary depletion regions has been studied. Figure 2(a) shows an SIM map obtained on a large region of a sample showing a grain size distribution from ~1 up to ~10 μm in diameter. The SIM image shows that the width of the grain boundary depletion regions is almost independent of the grain dimensions. Figure 2(b) shows an SIM high resolution image of a single CCTO grain ~6 μm wide. At the center of the grain, two regions having different electrical behaviors have been observed: a darker ring surrounds a spot having a lighter contrast that is very similar to the main part of the grain. Figure 2(c) shows the current-voltage (I-V) characteristics performed by stopping the conductive atomic force microscopy (C-AFM) tip on both the dark ring (blue curve) and the light circle (red curve). The current flowing through the light region is two orders of magnitude higher than that through the dark ring. This indicates that the dark ring possesses a resistance two orders of magnitude higher and this signal is comparable with the resistance shown by the depletion regions at the grain boundaries. Thus, a conductive domain surrounded by insulating blocking areas has been found as a subgrain feature which influences the electrical microstructure of the CCTO ceramics.

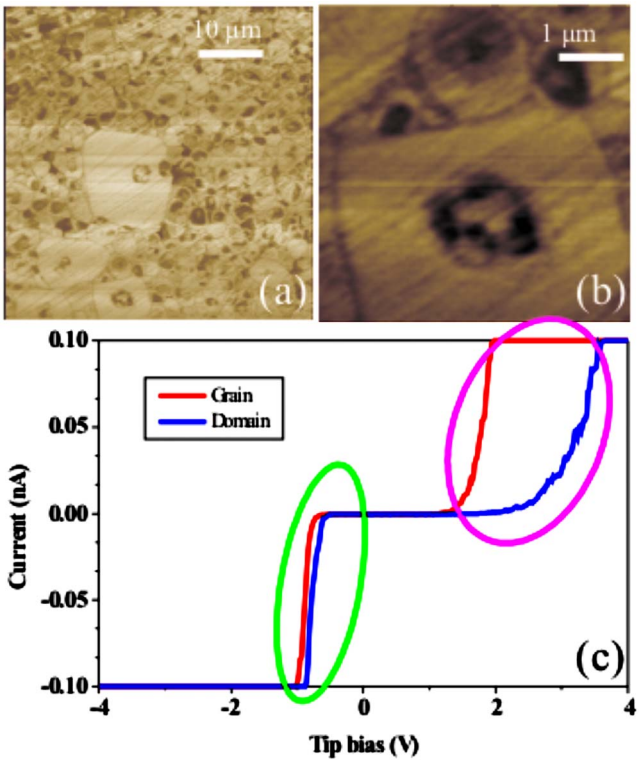

FIG. 2. (Color online) (a) SIM image of a polycrystalline CCTO sample with a wide grain size distribution. (b) High resolution SIM image of the insulating secondary-phase inclusion within a single CCTO grain. (c) I-V measurements collected by C-AFM on the light grain (blue curve) and on the dark domain (red curve), respectively.

Usually, polycrystalline materials can be described as a sequence of parallel (RC) elements connected in series. In the classic version of the brick-work layer model, one RC element can be related to the grains and another to the grain boundaries for which the impedance can be expressed as

$$Z^* = (R_g^{-1} + i\omega C_g)^{-1} + (R_{gb}^{-1} + i\omega C_{gb})^{-1} = \mathrm{Re}(Z^*) - i\,\mathrm{Im}(Z^*), \tag{3}$$

where

$$\mathrm{Re}(Z^*) = \frac{R_g}{1 + (\omega R_g C_g)^2} + \frac{R_{gb}}{1 + (\omega R_{gb} C_{gb})^2} \tag{4}$$

and

$$\mathrm{Im}(Z^*) = R_g\left[\frac{\omega R_g C_g}{1 + (\omega R_g C_g)^2}\right] + R_{gb}\left[\frac{\omega R_{gb} C_{gb}}{1 + (\omega R_{gb} C_{gb})^2}\right], \tag{5}$$

where (R_g, R_{gb}) and (C_g, C_{gb}) are the resistance and capacitance of the grains and grain boundaries, respectively.

The behavior of the simulated circuit is in agreement with the experimental I-V curves reported in Fig. 2(c). In particular, our experimental I-V data [Fig. 2(c) (green circle)]

represent the *I-V* inverted characteristics of the tip/CCTO single grain contact when a negative voltage is applied to the tip, and are almost identical both on the conducting and on the insulating regions.

By contrast, when a positive voltage is applied to the tip [Fig. 2(c) (inside the magenta circle)], the collected data can be attributed to the inverted *I-V* characteristics of the barriers embedded within the CCTO single grain either due to the grain boundary depleted region or to the presence of an insulating precipitate. Consequently, the reported SIM maps are not affected by any superficial contribution or artifacts but by collected local information on the sample volume below the tip. The imaging of insulating regions within conductive grains also reveals compositional inhomogeneity within CCTO ceramics; if similar features exist in single crystals, this may provide a possible further explanation for the observed giant permittivity effect.

In this context, the standard equivalent circuit of two parallel RC elements connected in series (R_bC_b-$R_{gb}C_{gb}$) needs to be modified by adding a third parallel RC element (R_dC_d) that represents the insulating subgrain feature observed in this study. The complex impedance of this circuit is given by

$$Z^* = (R_g^{-1} + i\omega C_g)^{-1} + (R_{gb}^{-1} + i\omega C_{gb})^{-1} + (R_d^{-1} + i\omega C_d)^{-1}$$
$$= \mathrm{Re}(Z^*) - i\,\mathrm{Im}(Z^*). \quad (6)$$

The results of conventional impedance spectroscopy studies on CCTO ceramics show that $C_g \ll C_{gb}$ and $R_g \ll R_{gb}$. Comparing our SIM and C-AFM data, no difference has been found, thus, indicating that the impedance variation in the domains is basically due to resistance variations. The *I-V* measurements have shown that $R_d \approx R_{gb} >> R_g$ and it is reasonable to suppose that $C_d \approx C_{gb} >> C_g$. It is therefore possible to suggest that the presence of R_dC_d may give rise to a dielectric anomaly in single crystals and may, at least in part, explain the giant permittivity reported for CCTO crystals.

The chemical nature of the insulating domains within the CCTO grains has been evaluated by energy filtered transmission electron microscopy. Figure 3(a) shows a TEM micrograph within a CCTO single grain. A crystalline domain about 200 nm wide is clearly visible. The Ti [Fig. 3(b)], Ca [Fig. 3(c)], and Cu [Fig. 3(d)] elemental maps indicate that the domain is Cu-free and consists of a calcium titanate phase.

Thus, the presence of insulating precipitates may contribute to raising the overall permittivity of CCTO ceramics and provide a possible explanation of the CCTO single crystal response.

In conclusion, SIM has been demonstrated to image the electrical properties of CCTO ceramics with high lateral resolution. This technique allowed the electrical characterization of subgrain microstructural features in addition to the usual grain boundary characterization which can be obtained from conventional techniques, such as impedance spectroscopy. SIM has revealed the presence of depletion regions, which are ~130 nm in width, at the grain boundaries which confirms the applicability of an IBLC-type model to explain the electrical properties of CCTO ceramics. The width of the grain boundary depletion regions appears to be independent of the applied voltage and grain dimensions. Energy Filtered (EFTEM) analysis revealed the presence of subgrain features associated with the insulating secondary phase inclusions,

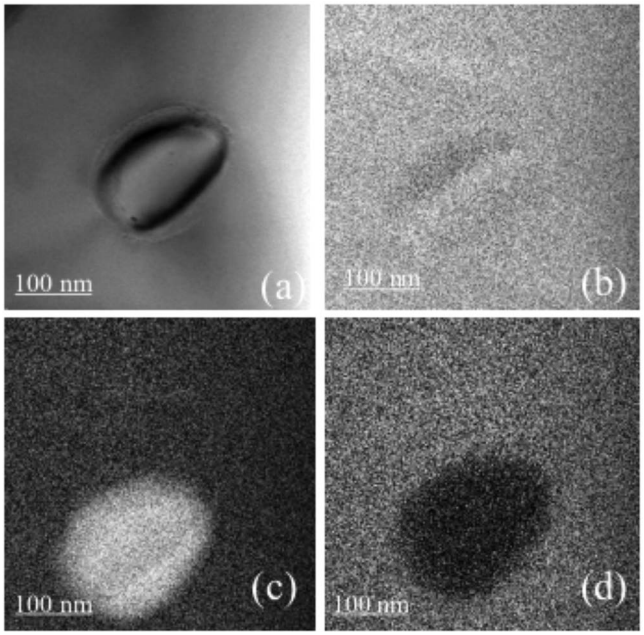

FIG. 3. (a) TEM image of an inclusion within CCTO grain. EFTEM maps of the (b) titanium, (c) calcium, and (d) copper. They indicate that it consists of a copper-free calcium titanate phase.

which are observed by SIM within individual grains. The secondary phase can block/restrict conduction within individual grains provided that the current is unable to bypass the second phase and, if present, CCTO crystals can contribute to the high measured permittivities. Finally, the experimental approach presented here could be used to investigate the dielectric properties of a wide class of inhomogeneous materials.

This work has been supported by European Union under the Project NUOTO (New Materials with Ultrahigh *k* dielectric constant fOr TOmorrow wireless electronics) Grant No. NMP3-CT-2006-032644.

[1] M. A. Subramanian, D. Li, N. Duan, B. A. Reisner, and A. W. Sleight, J. Solid State Chem. **151**, 323 (2000).
[2] C. C. Homes, T. Vogt, S. M. Shapiro, S. Wakimoto, and A. P. Ramirez, Science **293**, 217 (2001).
[3] J. Wu, C.-W. Nan, Y. Lin, and Y. Deng, Phys. Rev. Lett. **89**, 217601 (2002).
[4] B. Benner, P. Lunkenheimer, M. Schetter, A. Loidl, A. Reller, and S. G. Ebbinghaus, J. Appl. Phys. **96**, 4400 (2004).
[5] P. Lunkenheimer, V. Bobnar, A. V. Pronin, A. I. Ritus, A. A. Volkov, and A. Loidl, Phys. Rev. B **66**, 052105 (2002).
[6] T. B. Adams, D. C. Sinclair, and A. R. West, Adv. Mater. (Weinheim, Ger.) **14**, 1321 (2002).
[7] T. B. Adams, D. C. Sinclair, and A. R. West, Phys. Rev. B **73**, 094124 (2006).
[8] S. F. Shao, J. L. Zhang, P. Zheng, W. L. Zhang, and C. L. Wang, J. Appl. Phys. **99**, 084106 (2006).
[9] D. C. Sinclair, T. B. Adams, F. D. Morrison, and A. R. West, Appl. Phys. Lett. **80**, 2153 (2002).
[10] M. H. Cohen, J. B. Neaton, L. He, and D. Vanderbilt, J. Appl. Phys. **94**, 3299 (2003).
[11] P. Fiorenza, R. Lo Nigro, V. Raineri, R. G. Toro, and M. R. Catalano, J. Appl. Phys. **102**, 116103 (2007).
[12] G. Zang, J. Zhang1, P. Zheng, J. Wang, and C. Wang, J. Phys. D **38**, 1824 (2005).
[13] I.-D. Kim, A. Rothschild, and H. L. Tuller, Appl. Phys. Lett. **88**, 072902 (2006).
[14] J. Wu, C.-W. Nan, Y. Lin, and Y. Deng, Phys. Rev. Lett. **89**, 217601 (2002).
[15] T.-T. Fang and C. P. Liu, Chem. Mater. **17**, 5167 (2005).
[16] L. He, J. B. Neaton, M. H. Cohen, D. Vanderbilt, and C. C. Homes, Phys. Rev. B **65**, 214112 (2002).